Low-Temperature Synthesis of CoO Nanoparticles via Chemically Assisted Oxidative Decarbonylation

Anna Lagunas,[†] Antoni Mairata i Payeras,[†] Ciril Jimeno,[†] Víctor F. Puntes,[§,||] and Miquel A. Pericàs*[,†,‡]

Institute of Chemical Research of Catalonia, Avgda. Països Catalans, 16. E-43007 Tarragona, Spain, Departament de Química Orgànica, Universitat de Barcelona, E-08028 Barcelona, Spain, Institut Català de Nanotecnologia, Campus de Bellaterra, E-08193 Bellaterra, Spain, and Institut Català de Recerca i Estudis Avançats, Barcelona, Spain

Received July 16, 2007. Revised Manuscript Received October 15, 2007

A low-temperature route to pure CoO nanoparticles based on the oxidative decarbonylation of dicobalt octacarbonyl promoted by amine oxides is presented. The small size of the resulting particles (∼1.7 nm) leads to spontaneous nanoparticle aggregation. Magnetic measurements show a bimodal behavior with two distinct blocking temperatures, which can be ascribed to the individual CoO nanoparticles and to narrowly size-dispersed aggregates.

Introduction

Metalcarbonyls and metal–carbonyl complexes represent one of the most employed sources of reactive metallic species either in homogeneous catalysis[1] or for the controlled release of metal atoms in the synthesis of nanoparticles.[2,3] In general, CO dissociation from the metal atom in the starting complex can be induced in four general ways: (i) thermolysis,[3] (ii) sonolysis,[2] (iii) photolysis,[4] and (iv) by chemical assistance.[5,6]

In the context of the development of new, chemically assisted procedures for the decarbonylation of metal–carbonyl complexes, we have recently shown that TEMPO (2,2,6,6-tetramethylpiperidinoxyl radical), a stable free radical, is able to promote the decarbonylation of dicobalt hexacarbonyl complexes of alkynes through single-electron activation of cobalt−carbonyl bonds and that this behavior can efficiently trigger the Pauson−Khand cyclopentenone annulation.[7] We have subsequently shown that TEMPO can also promote the low-temperature decarbonylation of dicobalt octacarbonyl and that this process, when performed in the presence of appropriate additives, yields pure CoO nanoparticles in the form of monodisperse aggregates.[8]

Scheme 1. *N*-Oxide-Promoted Oxidative Decarbonylation/Oxidation of $Co_2(CO)_8$ Yielding Cobalt Oxide Colloidal Nanoparticles (CoO-CNP)

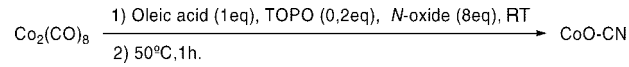

Because it is well-known that amine oxides are also able to promote the decarbonylation of metal–carbonyl complexes under mild conditions and because this property has been widely used with synthetic purposes,[9] we thought that the amine oxide-induced decarbonylation of dicobalt octacarbonyl could also be an efficient procedure for nanoparticle formation.

The reactivity of *N*-oxides toward metal–carbonyls mentioned above was first observed by Hieber and Lipp,[10] who reported that $Fe(CO)_5$ reacted with pyridine *N*-oxide to form pyridine and iron oxides. It was soon established that trimethylamine *N*-oxide (TMAO), a more powerful oxidizing agent, was able to induce the decarbonylation under milder reaction conditions,[11] and the process began to be used with synthetic purposes.[12] Later, it was shown that this mild decarbonylation method can be applied to other metal–carbonyl complexes[13] and that it represents a most convenient method for the synthesis of substituted metal–carbonyl

* To whom correspondence should be addressed. E-mail: mapericas@iciq.es. Fax: (+34) 977 920 222.
† Institute of Chemical Research of Catalonia (ICIQ).
‡ Universitat de Barcelona (UB).
§ Institut Català de Nanotecnologia (ICN).
|| Institut Català de Recerca i Estudis Avançats (ICREA).

(1) *Applied Homogeneous Catalysis with Organometallic Compounds.*, 2nd ed.; Cormils, B., Herrmann, W. A., Eds; Wiley-VCH: Weinheim, Germany, 2002; *Vol. 1–3*.
(2) Mastai, Y.; Gedanken, A. *Sonochemistry and Other Novel Methods Developed for the Synthesis of Nanoparticles, in The Chemistry of Nanomaterials*; Rao, C. N. R., Müller, A., Cheetham, A. K., Eds; Wiley-VCH: Weinheim, Germany, 2004; Vol. 1, p 113.
(3) (a) Puntes, V. F.; Krishnan, K. M.; Alivisatos, A. P. *Science* **2001**, *291*, 2115. (b) Puntes, V. F.; Zanchet, D.; Erdonmez, C. K.; Alivisatos, A. P. *J. Am. Chem. Soc.* **2002**, *124*, 12874.
(4) Szyma'nska-Buzar, T. *Coord. Chem. Rev.* **2006**, *250*, 976.
(5) Shen, J.-K.; Gao, Y.-C.; Shi, Q.-Z.; Basolo, F. *Coord. Chem. Rev.* **1993**, *128*, 69.
(6) (a) For a review on reaction mechanisms of chemically assisted synthesis of nanoparticles, see: Niederberger, M.; Garnweitner, G. *Chem.−Eur. J.* **2006**, *12*, 7282. (b) For some additional examples, see: Banerjee, S.; Santhanam, A.; Dhathathreyan, A.; Rao, P. M. *Langmuir* **2003**, *19*, 5522. (c) Kanthimathi, M.; Dhathathreyan, A.; Nair, B. U. *Mater. Lett.* **2004**, *58*, 2914.
(7) Lagunas, A.; Mairata i Payeras, A.; Jimeno, C.; Pericàs, M. A. *Org. Lett.* **2005**, *7*, 3033.
(8) Lagunas, A.; Mairata i Payeras, A.; Jimeno, C.; Pericàs, M. A. *Chem. Commun.* **2006**, 1307.
(9) *Transition Metals for Organic Synthesis*, 2nd ed.; Beller, M., Bolm, C., Eds.; Wiley-VCH: Weinheim, Germany, 2004; Vol *1–2*.
(10) Hieber, W.; Lipp, A. *Chem. Ber.* **1959**, *92*, 2085.
(11) Black, D. S. C.; Deacon, G. B.; Thomas, N. C. *Inorg. Chim. Acta* **1982**, *65*, L75.
(12) Shvo, Y.; Hazum, J. *J. Chem. Soc., Chem. Commun.* **1975**, 829.
(13) Eekhof, J. H.; Hogveen, H.; Kellogg, R. M. *J. Chem. Soc., Chem. Commun.* **1976**, 657.

10.1021/cm7018636 CCC: $40.75
Published on Web 11/20/2007

clusters.[14] More recently, Hyeon et al. took advantage of this chemistry and prepared different types of γ-Fe_2O_3 nanoparticles, either by oxidizing iron nanoparticles or by oxidative decomposition of $Fe(CO)_5$ at 120 °C.[15]

Transition metal oxide nanocrystals are the subject of increasing interest because of their fundamental properties and technological applications.[16] In particular, CoO nanoparticles can be used as catalyst precursors,[17] to prepare pigments,[18] or as an anisotropy source for magnetic recording.[19]

Pure CoO nanoparticles are difficult to prepare by oxidative procedures because of the greater thermodynamical stability of Co_3O_4.[20] Despite these problems, the methods described in the literature for the synthesis of highly crystalline and size-controlled CoO nanoparticles generally imply harsh reaction conditions (including high temperatures and long reaction times starting from a broad variety of precursors).[21] In fact, in addition to our recently reported approach to this class of nanoparticles,[8] only Chaudret et al. have succeeeded in preparing nanometric CoO particles through a low-temperature approach. These authors prepared CoO nanoparticles dispersed in a polymer matrix by solid-state, room-temperature, air oxidation of the metallic colloid precursor. However, the oxidation was not always complete, and it took considerably long periods of time.[22] It is thus of high practical interest to develop mild and efficient methods to prepare this type of nanoparticle.

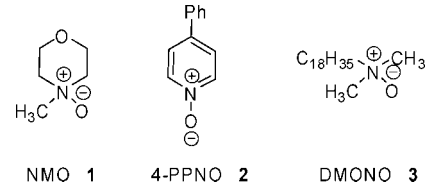

Figure 1. Structures of the *N*-oxides used for CoO nanoparticle synthesis.

Scheme 2. Proposed Mechanism for CO/R_3N Substitution on a Mononuclear Metal–Carbonyl via *N*-Oxide Mediated CO Oxidation

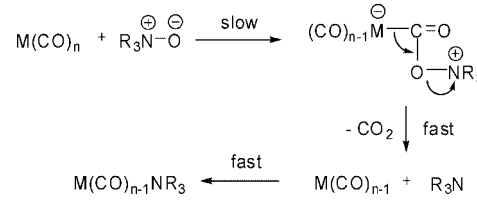

In this paper, we report that the room-temperature, amine oxide-mediated oxidation of $Co_2(CO)_8$ leads to pure CoO nanoparticles of small size (~1.7 nm) that spontaneously agglomerate into narrowly disperse aggregates. We also show that the nature of the amine oxide used in the process affects the characteristics of the obtained nanoparticles, especially their magnetic properties.

Experimental Section

General. Reactions were performed in flame-dried flasks under argon atmosphere. *o*-Dichlorobenzene was degassed prior to use. Anhydrous dichloromethane was obtained from a Solvent Purification System. Trioctylphosphine oxide, oleic acid, *N*-methylmorpholine *N*-oxide (NMO), and 4-phenylpyridine *N*-oxide (PPNO) were obtained from commercial sources and were employed as received. *N,N*-Dimethyloctadecylamine *N*-oxide (DMONO) was prepared by oxidation of *N,N*-dimethyloctadecylamine by a reported procedure.[23]

Synthesis of CoO Nanoparticles. In a typical experiment, 0.500 g (1.46 mmol) of $Co_2(CO)_8$ and 105 mg (0.272 mmol) of trioctylphosphine oxide (TOPO) were dissolved in anhydrous *o*-dichlorobenzene (20 mL) under argon. Then, 0.5 mL (0.445 g, 1.58 mmol) of oleic acid were added. Next, a solution of 8 equiv (11.68 mmol) of the corresponding *N*-oxide in anhydrous dichloromethane (PPNO, DMONO) or in a 1:1 mixture of dichloromethane and *o*-dichlorobenzene (NMO) was slowly added via syringe to the reaction mixture at the selected temperature (room temperature (RT) or below). The reaction mixture was then heated at 50 °C for 1 h, and after the mixture was cooled to room temperature, 10 mL of acetone was added. The resulting suspension was centrifuged at 4400 rpm for 1 h, and the precipitate of CoO nanoparticles was washed two times with dichloromethane and dried at room temperature under a mild nitrogen stream.

Characterization. For transmission electron microscopy (TEM) studies, one drop of a diluted suspension of the particles in hexane was placed on a carbon coated holey Formvar copper grid (200 mesh). A Hitachi 800MT Transmission Electron Microscopy (200 keV) provided with a Gatan Multiscan chamber was used to obtain low-resolution micrographs. For high-resolution images and for selected-area electron diffraction analysis (SAED), a Philips CM30 LaB6 microscope operated at

(14) (a) Johnson, B. G. F.; Lewis, J.; Pippard, D. *J. Organomet. Chem.* **1978**, *160*, 263. (b) Stunz, G. F.; Shapley, J. R. *J. Organomet. Chem.* **1981**, *213*, 389. (c) Luh, T. Y. *Coord. Chem. Rev.* **1984**, *60*, 255.
(15) Hyeon, T.; Lee, S. S.; Park, J.; Chung, Y.; Na, H. B. *J. Am. Chem. Soc.* **2001**, *123*, 12798.
(16) Seshadri, R. Oxide Nanoparticles. In *The Chemistry of Nanomaterials*; Rao, C. N. R., Müller, A., Cheetham, A. K., Eds.; Wiley-VCH: Weinheim, Germany, 2004; Vol. 1, p 94.
(17) (a) Bezemer, G. L.; Bitter, J. H.; Kuipers, H. P. C. E.; Oosterbeek, H.; Holewijn, J. E.; Xu, X.; Kapteijn, F.; van Dillen, A. J.; de Jong, K. P. *J. Am. Chem. Soc.* **2006**, *128*, 3956. (b) Dry, M. E. *Catal. Today* **2002**, *71*, 227.
(18) (a) Feldmann, C. *Adv. Mater.* **2001**, *13*, 1301. (b) Feldmann, C.; Jungk, H.-O. *Angew. Chem., Int. Ed.* **2001**, *40*, 359.
(19) (a) Nogú; es, J.; Skumryev, V.; Sort, J.; Stoyanov, S.; Givord, D. *Phys. Rev. Lett.* **2006**, *97*, 157203. (b) Skumryev, V.; Stoyanov, S.; Zhang, Y.; Hadjipanayis, G.; Givord, D.; Nogués, J. *Nature* **2003**, *423*, 850. (c) Tomou, A.; Gournis, D.; Panagiotopoulosa, I.; Huang, Y.; Hadjipanayis, G. C.; Kooi, B. J. *J. Appl. Phys.* **2006**, *99*, 123915. (d) Tracy, J. B.; Weiss, D. N.; Dinega, D. P.; Bawendi, M. G. *Phys. Rev. B.* **2005**, *72*, 064404.
(20) (a) Wang, Z. L.; Yin, J. S.; Mo, W. D.; Zhang, Z. J. *J. Phys. Chem. B* **1997**, *101*, 6793. (b) Soriano, L.; Abbate, M.; Fernández, A.; González-Elipe, A. R.; Sirotti, F.; Sanz, J. M. *J. Phys. Chem. B.* **1999**, *103*, 6676. (c) Yin, J. S.; Wang, Z. L. *Phys. Rev. Lett.* **1997**, *79*, 2570.
(21) (a) Zhang, Y.; Zhong, X.; Zhu, J.; Song, X. *Nanotechnology* **2007**, *18*, 19605. (b) Narayanaswamy, A.; Xu, H.; Pradhan, N.; Peng, X. *Angew. Chem., Int. Ed.* **2006**, *45*, 5361. (c) An, K.; Lee, N.; Park, J.; Kim, S. C.; Hwang, Y.; Park, J.-G.; Kim, J.-Y.; Park, J.-H.; Han, M. J.; Yu, J.; Hyeon, T. *J. Am. Chem. Soc.* **2006**, *128*, 9753. (d) Park, J.; An, K.; Hwang, Y.; Park, J.-G.; Noh, H.-J.; Kim, J.-Y.; Park, J.-H.; Hwang, N.-M.; Hyeon, T. *Nat. Mater.* **2004**, *3*, 891. (e) Ye, Y.; Yuan, F.; Li, S. *Mater. Lett.* **2006**, *60*, 3175. (f) Sun, X.; Zhang, Y.-W.; Si, R.; Yan, C.-H. *Small* **2005**, *1*, 1081. (g) Ghosh, M.; Sampathkumaran, E. V.; Rao, C. N. R. *Chem. Mater.* **2005**, *17*, 2348. (h) Seo, W. S.; Shim, J. H.; Oh, S. J.; Lee, E. K.; Hur, N. H.; Park, J. T. *J. Am. Chem. Soc.* **2005**, *127*, 6188. (i) Risbud, A. S.; Snedecker, L. P.; Elcombe, M. M.; Cheetham, A. K.; Seshadri, R. *Chem. Mater.* **2005**, *17*, 834. (j) Zhang, L.; Xue, D. *J. Mater. Sci. Lett.* **2002**, *21*, 1931. (k) Xu, C.; Liu, Y.; Xu, G.; Wang, G. *Chem. Phys. Lett.* **2002**, *366*, 567.
(22) Verelst, M.; Ely, T. O.; Amiens, C.; Snoeck, E.; Lecante, P.; Mosset, A.; Respaud, M.; Broto, J. M.; Chaudret, B. *Chem. Mater.* **1999**, *11*, 2702.
(23) *Org. Synth.* **1963**, *4*, 612.

300 keV was employed. Electron energy loss spectroscopy (EELS) analysis was performed on a Jeol JEM 2010F instrument equipped with a high-resolution digitalizing chamber at 200 keV and with a field emission gun. EELS was performed using a Gatan image filter (GIF).

Magnetic measurements on the solid samples were collected in a Quantum Design MPMS SQUID magnetometer (AC and DC modes and maximum static field of ±5 T) in liquid helium, after it was cooled in zero magnetic field (zero-field cooling, ZFC) or in a field of 50 Oe (field cooling, FC).

The X-ray photoelectron spectroscopy (XPS) spectra were recorded in a Perkin-Elmer PHI 5500 spectrophotometer using the Mg Kα radiation source. In depth measurements were obtained by recording the spectra after sputtering the samples to different depths with an Ar^+ ion beam at 4 keV.

Thermogravimetric analysis was carried out in a Mettler thermo balance, SDTA851e model, with a precision of ±0.25% and 1600 °C maximum temperature.

Online IR experiments were performed in a ReactIR 4000 (Mettler-Toledo AutoChem ReactIRTM) with a silicon probe (SiComp, optical range = 4400–650 cm^{-1}).

X-Ray Diffraction analyses were done in a Bragg–Brentano $\theta/2\theta$ geometry Siemens D-500 S2 powder diffractometer.

Results

Synthesis of CoO Nanoparticles. When a solution of $Co_2(CO)_8$ in *o*-dichlorobenzene, containing oleic acid and trioctylphoshine oxide (TOPO) as additives, was treated with a large excess (8 equiv) of amine oxides **1–3** (Scheme 1), an immediate evolution of carbon dioxide was observed. Very interestingly, the decarbonylation reaction took place at room temperature or below in just a few minutes, as was evident from the release of gas during the reaction and from in situ ATR-FTIR monitoring (see below).

Treatment of the resulting solution with acetone and subsequent centrifugation led to the isolation of a solid residue that could be characterized as oleic acid-coated, small CoO nanoparticles (~1.7 nm diameter), agglomerated into spherical aggregates.

From an operational point of view, a curing period of one hour at 50 °C was normally introduced before isolation of the final nanocolloid because it was observed that this resulted in an increased yield of CoO nanoparticles. However, neither the size of the individual particles or the shape or size of the aggregates was essentially modified by this treatment.

The *N*-oxides tested as mediators in the synthesis are shown in Figure 1. *N*-Methylmorpholine *N*-oxide (NMO, **1**) and 4-phenylpyridine *N*-oxide (4-PPNO, **2**) are common organic oxidizing agents usually employed in organic synthesis, NMO being considered as a stronger oxidant than 4-PPNO. *N,N*-Dimethyloctadecylamine *N*-oxide (DMONO, **3**), in turn, should possess oxidizing power similar to that of NMO and was chosen because of the nature of the proposed amine oxide-mediated mechanism for ligand substitution on metal–carbonyls (see Scheme 2).[24] Thus, we wanted to explore the possibility that the long-chain tertiary amine, formed from the amine oxide as a coproduct, could coordinate to the surface cobalt atoms in the product particles, acting as a competing stabilizing agent (in addition to oleic acid, TOPO, or both) and exert some influence on the nanoparticle topology.

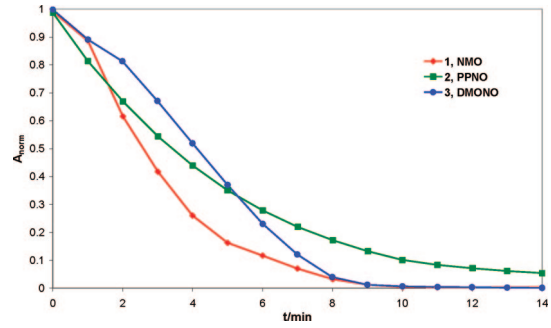

Figure 2. ATR-FTIR monitoring of the carbonyl band at 2022 cm^{-1} in the decarbonylation of $Co_2(CO)_8$ with different *N*-oxides.

In this respect, it is to be noted that the nanoparticle topology can be strongly influenced by the nature of the surfactants used for their stabilization. A clear example of this behavior can be found in cobalt nanoparticles, whose crystalline phase,[25] shape,[3b] and even, mechanism of formation[26] are controlled by the surfactants.

In practice, with the use of DMONO, the whole process for CoO nanoparticle synthesis could be carried out at −10 °C, while with NMO or 4-PPNO, it was necessary to work at room temperature or above.

In situ attenuated total reflectance FTIR (ATR-FTIR) monitoring of the reactions at room temperature was carried out to ensure that the decarbonylation process was complete and to obtain kinetic information on the process (see Supporting Information (SI) for the experimental setup). This sensitive technique enables the performance of selective detection of the species in solution which are in direct contact with the probe window and, therefore, only the soluble precursor species are detected.[26] To perform these experiments, an initial concentration of 0.050 g/mL of $Co_2(CO)_8$ was used in all cases, and the addition rate of the solution containing the *N*-oxide was fixed at 0.2 mL/min using a syringe pump. The profile obtained from the signal at 2022 cm^{-1} (Figure 2), corresponding to the stretching of terminal cobalt-bonded carbonyl ligands in the soluble precursor or in reaction intermediates was used to monitor the evolution of the decarbonylation process.

Clearly, different decarbonylation rates were observed for the three *N*-oxides, with NMO and DMONO promoting

(24) ShiY. L.; Gao, Y. C.; ShiQ. Z.; Kershner, D. L.; Basolo, F. *Organometallics* **1987**, *6*, 1528, (Correction: *Organometallics*, **1988**, *7*, 1234). (b) Gao, Y. C.; Shi, Q. Z.; Kershner, D. L.; Basolo, F. *Inorg. Chem.* **1988**, *27*, 188. (c) Shen, J. K.; Shi, Y. L.; Gao, Y. C.; Shi, Q. Z.; Basolo, F. *J. Am. Chem. Soc.* **1988**, *110*, 2414. (d) Shen, J. K.; Gao, Y. C.; Shi, Q. Z.; Basolo, F. *Inorg. Chem.* **1988**, *27*, 4236. (e) Shen, J. K.; Gao, Y. C.; Shi, Q. Z.; Basolo, F. *Organometallics* **1989**, *8*, 2144.
(25) Dinega, D. P.; Bawendi, M. G *Angew. Chem., Int. Ed.* **1999**, *38*, 1788.
(26) Lagunas, A.; Jimeno, C.; Font, D.; Solà, L.; Pericàs, M. A. *Langmuir* **2006**, *22*, 3823.

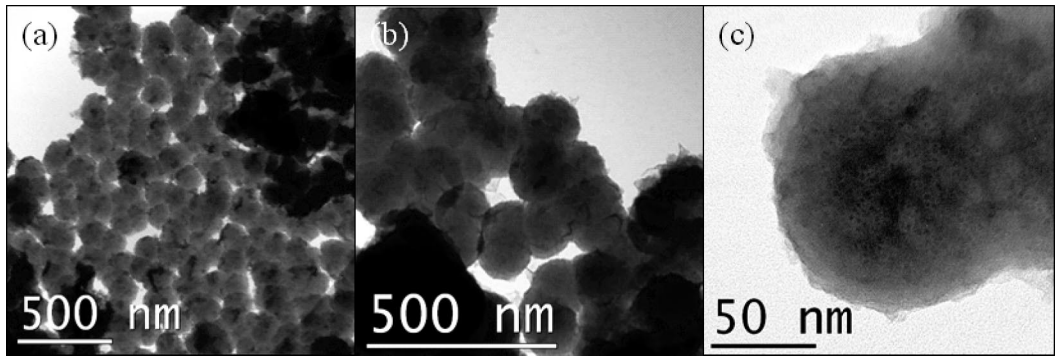

Figure 3. TEM images of the aggregates of CoO nanoparticles obtained with NMO at different magnifications. Small CoO particles inside the aggregate can be distinguished in picture (c) as dark spots.

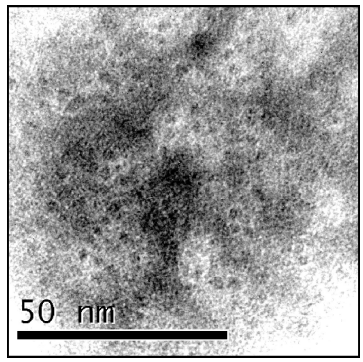

Figure 4. TEM image of CoO nanoparticles prepared with NMO at higher magnification showing the individual constituent nanoparticles.

faster reactions than PPNO (Figure 2). The decarbonylation of $Co_2(CO)_8$ was complete in 9–10 min with NMO and DMONO, whereas it took more than 15 min with PPNO. Thus, these data fully confirm the intuitive idea on the relative oxidizing power of the three considered amine oxides.

Characterization. The overview TEM image of the particles synthesized by decarbonylation/oxidation with **1** (Figure 3) showed an aggregate-type structure.[27] The magnified image presented in Figure 4 shows individual CoO particles, of ~1.7 nm diameter ($s = 0.5$ nm), embedded in one of those aggregates.[28] The microstructure of the other samples prepared with **2** and **3** is described in the SI.

When the size distribution of the aggregates is statistically analyzed, fitting to a log-normal distribution for $n = 30$, in all cases, leads to a mean aggregate diameter of 113 nm ($s = 11$ nm) for the CoO nanoparticles prepared by oxidation with NMO, 155 nm ($s = 18$ nm) mean aggregate diameter for the particles prepared with PPNO, and 156 nm ($s = 32$ nm) mean aggregate diameter for particles prepared with DMONO (**3**). Therefore, the diameter of the aggregates depends on the employed amine oxide. The microstructural characterization however shows similar results in the three cases, while magnetic characterization shows more differences between the samples.

Selected area electron diffraction (SAED) performed on samples of isolated nanoparticles aggregates (Figure 5) exhibited a concentric ring structure indicating a polycrystalline material. Interestingly, this structure appears to be quite diffuse, what correspond to very small crystal domains. Comparison of the *d*-spacing distances from the diffraction pattern with those indexed for cobalt- and cobalt−oxygen-containing compounds,[29] allows the assignment of the structure as face-centered cubic CoO with the *Fm3m* space group (see Figure 5a).

Similar results are observed with the X-ray diffraction (XRD) analysis of the material (Figure 5b), where very broad peaks are observed, consistent with CoO diffraction patterns of very small particles.[21b] In fact, for particles smaller than 3 nm the crystal periodicity is so reduced that the interference phenomena that underlays X-ray crystal diffraction starts disappearing.

To better assess the chemical nature of the nanoparticles prepared in the present study, spectroscopic techniques such as XPS and EELS were also employed (Figure 6). The XPS spectrum of the CoO nanoparticles synthesized using NMO is shown in Figure 6a. Identical spectra were recorded for the samples of nanoparticles prepared with the other studied *N*-oxides (see Supporting Information).

The peak at 780.8 eV is from Co $2p_{3/2}$, with a shakeup satellite at 785.9 eV, while the peak at 797.2 eV is caused by Co $2p_{1/2}$, with a satellite peak at 803.0 eV. The presence of those two peaks and the highly intense satellites near them is consistent with the presence of Co^{2+} in the high-spin state. The absence of a signal at 778.1 eV indicates the nonexistence of Co metal impurities.[21b]

(27) (a) For selected examples of well-defined nanoparticles aggregates, see: Ye, E.; Tan, H.; Li, S.; Fan, W. Y. *Angew. Chem., Int. Ed.* **2006**, *45*, 1120. (b) Zhou, S.; McIlwrath, K.; Jackson, G.; Eichhorn, B. *J. Am. Chem. Soc.* **2006**, *128*, 1780. (c) Zhou, X.; Chen, S.; Zhang, D.; Guo, X.; Ding, W.; Chen, Y. *Langmuir* **2006**, *22*, 1383. (d) Hussain, I.; Wang, Z.; Cooper, A. I.; Brust, M. *Langmuir* **2006**, *22*, 2938. (e) Jin, J.; Iyoda, T.; Cao, C.; Song, Y.; Jiang, L.; Li, T. J.; Zhu, D. B. *Angew. Chem., Int. Ed.* **2001**, *40*, 2135. (f) Ely, T. O.; Amiens, C.; Chaudret, B. *Chem. Mater.* **1999**, *11*, 526.

(28) In the case of nanoparticles prepared with PPNO or DMONO (see Supporting Information), the aggregates exhibited a similar structure, but less well defined in shape and size. Thus, although aggregates of CoO nanoparticles are obtained in all cases, NMO proved to be the best promoter in terms of product yield and morphology.

(29) (a) Rask, J. H.; Mine, B. A.; Buseck, P. R. *Ultramicroscopy.* **1987**, *32*, 319. (b) Pearson, D. H.; Ahn, C. C.; Fultz, B. *Phys. Rev. B.* **1993**, *47*, 8471. (c) Pearson, D. H.; Fultz, B.; Ahn, C. C. *Appl. Phys. Lett.* **1988**, *53*, 1405. (d) Kurata, H.; Colliex, C. *Phys. Rev. B.* **1993**, *48*, 2102. (e) Pease, D. M.; Bader, S. D.; Brodsky, M. B.; Budnick, J. I.; Morrison, T. I.; Zaluzec, N. J. *Phys. Lett.* **1986**, *114A*, 491. (f) Morrison, T. I.; Brodsky, M. B.; Zaluzec, N. J.; Sill, L. R. *Phys. Rev. B.* **1985**, *32*, 3107. (g) Mansot, J. L.; Leone, P.; Euzen, P.; Palvadeau, P. *Microsc., Microanal., Microstruct.* **1994**, *5*, 79. (h) Fortner, J. A.; Buck, E. C. *Appl. Phys. Lett.* **1996**, *68*, 3817.

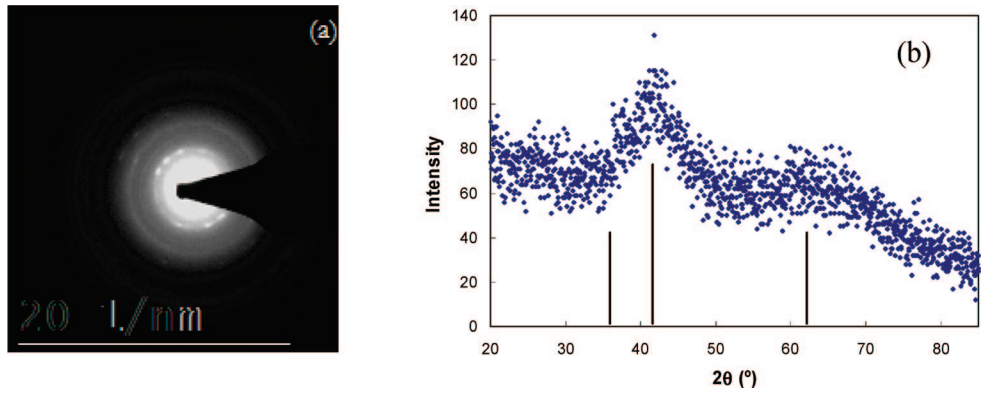

Figure 5. SAED and XRD of CoO nanoparticles (prepared with NMO). Inserted bars in the XRD correspond to predicted peaks for CoO.

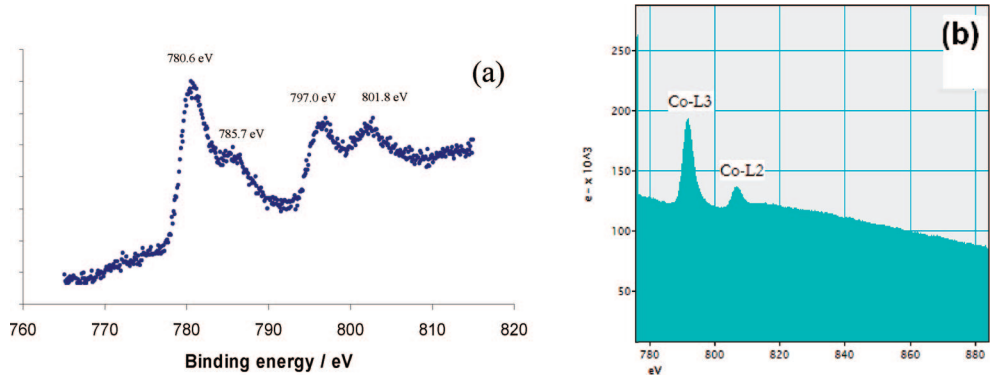

Figure 6. (a) Co 2p core-level XPS of CoO nanoparticles synthesized using NMO as a decarbonylation/oxidation agent. (b) EELS spectrum of CoO nanoparticles synthesized using DMONO as a decarbonylation/oxidation agent.

Similarly, the different samples of nanoparticles were studied in the electron microscope through electron energy-loss spectroscopy (EELS).[29] Numerous EELS experiments have shown that a change in valence states of cations introduces a dramatic change in the ratio of the white lines (L ionization edges) intensities, leading to the possibility of identifying the occupation number of 3d orbitals using this technique. After background removal and quantification of the area under the white line curves, L_3/L_2 can be calculated, resulting in 4.64 for the nanoparticles obtained by decarbonylation/oxidation with DMONO (Figure 6b). This ratio fits nicely with the published results with CoO.[20a] Similar results are obtained for the nanoparticles prepared with NMO and PPNO.

Discussion

Mechanistic Aspects of the Conversion of $Co_2(CO)_8$ into CoO. The role of amine oxides in the chemically induced decarbonylation of metal–carbonyl complexes has been well established since the pioneering work of Basolo.[24] Thus, it is known that amine oxides attack metal-bonded CO ligands promoting their oxidation to CO_2 and subsequent detachment from the metal center (Scheme 2). A sequence of such processes on a polycarbonyl complex like $Co_2(CO)_8$would lead to CO-depleted complexes, probably stabilized by labile trialkylamino ligands (eq 1).

$$Co_2(CO)_8 + nR_3N{-}O \rightarrow Co_2(CO)_{8-n}(R_3N)_n + nCO_2 \quad (1)$$

However, the formation of CoO in the process requires that the participating amine oxide also plays the role of oxidizing

Scheme 3. Plausible Mechanism for Co Oxidation with Amine Oxides via an Intermediate Aminoxy Complex

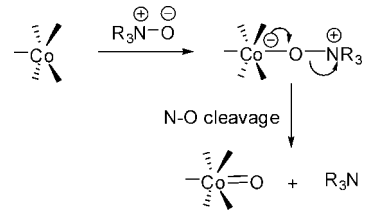

the cobalt atoms in the initial complex. While a mechanism for this process has not been proposed before, it is logical to assume that an amine oxide molecule can interact with a coordinatively unsaturated cobalt complex leading to a zwitterionic aminoxy complex (Scheme 3). A subsequent cleavage of the oxygen−nitrogen bond would lead to the generation of an oxidized Co species and a trialkylamine molecule.

To test the energetic requirements of this possibility, we decided to study the process by theoretical means on a model compound. Dicobalt heptacarbonyl was selected as the oxidation substrate, with trimethylamine *N*-oxide (TMAO) as the oxidant. The geometries of all the studied species were fully optimized with the semiempirical procedure PM3,[30] which incorporates parametrization for transition metals to the original PM3

(30) It has been shown that PM3(tm) reproduces well the structure and conformation of the closely related dicobalt hexacarbonyl complexes of alkynes as determined by X-ray crystallography. See: Verdaguer, X.; Vázquez, J.; Fuster, G.; Bernardes-Génisson, V.; Greene, A. E.; Moyano, A.; Pericàs, M. A.; Riera, A. *J. Org. Chem.* **1998**, *63*, 7037.

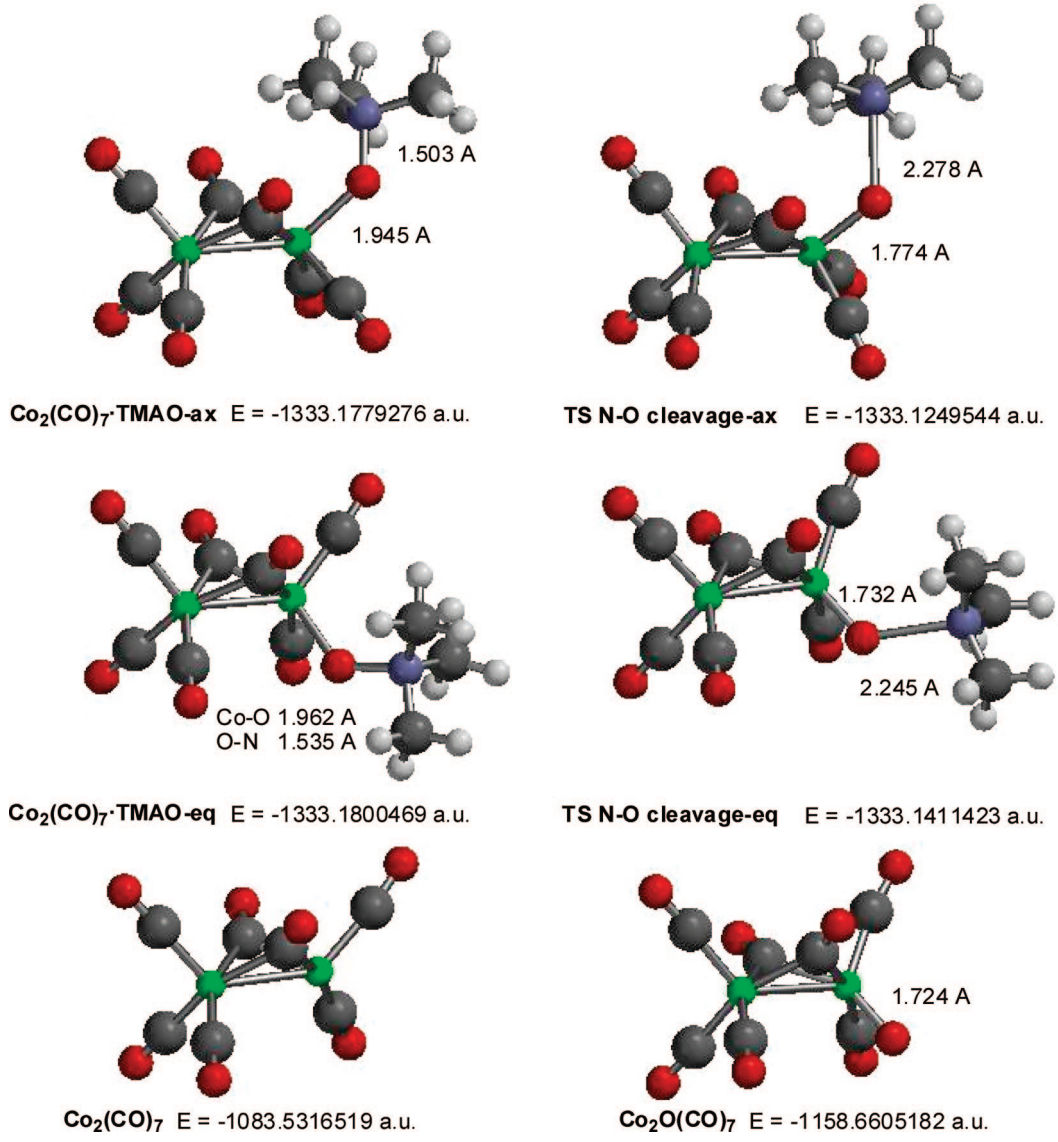

Figure 7. PM3-optimized structures and DFT-calculated energies for the relevant species in the oxidation of $Co_2(CO)_7$ mediated by TMAO.

procedure,[31] as implemented in the Spartan'02 suite of programs.[32] Single-point energy calculations were next performed on the optimized geometries using density functional theory (DFT) with the B3LYP functional. The LACVP* basis set, which includes Hay and Wadt's effective core potential for cobalt and is equivalent to a 6–31G* basis set for elements lighter than Ar was used in the calculations.[33,34]

We have summarized in Figure 7 the PM3-optimized structures and the DFT-calculated energies of the relevant intermediates and transition states located in this study.

First of all, it is interesting to note that the interaction between the coordinatively unsaturated $Co_2(CO)_7$ species and the amine oxide TMAO is predicted to be highly stabilizing ($\Delta E = -26.8$ kcal/mol). Thus, it is logical to expect that amine oxides, highly abundant in the reaction media during the complex process leading to CoO nanoparticles, will advantageously compete with other present Lewis bases (i.e., tertiary amines, TOPO, oleate, etc.) for available coordination sites on cobalt.

Two different structures were located for the $Co_2(CO)_7$-trimethylamine oxide adducts (**$Co_2(CO)_7$·TMAO-ax** and **$Co_2(CO)_7$·TMAO-eq**). They differ in the position (axial or equatorial) occupied by the TMAO ligand and, according to the known fluxional behavior of cobalt carbonyl complexes,[35] they should readily interconvert at room temperature. According to the calculated B3LYP energies, the

(31) Stewart, J. J. P. *J. Comput. Chem.* **1989**, *10*, 209.
(32) (a) *Spartan '02*; Wavefunction, Inc.: Irvine, CA, 2002. (b) Kong, J.; White, C. A.; Krylov, A. I.; Sherrill, D.; Adamson, R. D.; Furlani, T. R.; Lee, M. S.; Lee, A. M.; Gwaltney, S. R.; Adams, T. R.; Ochsenfeld, C.; Gilbert, A. T. B.; Kedziora, G. S.; Rassolov, V. A.; Maurice, D. R.; Nair, N.; Shao, Y.; Besley, N. A.; Maslen, P. E.; Dombroski, J. P.; Daschel, H.; Zhang, W.; Korambath, P. P.; Baker, J.; Byrd, E. F. C.; Van Voorhis, T.; Oumi, M.; Hirata, S.; Hsu, C.-P.; Ishikawa, N.; Florian, J.; Warshel, A.; Johnson, B. G.; Gill, P. M. W.; Head-Gordon, M.; Pople, J. A. *J. Comput. Chem.* **2000**, *21*, 1532.
(33) Hay, P. J.; Wadt, W. R. *J. Chem. Phys.* **1985**, *82*, 270.
(34) Markies, P. R.; Schat, G.; Akkerman, O. S.; Bickelhaupt, F. *Organometallics* **1990**, *9*, 2243.
(35) (a) Aime, S.; Milone, L.; Sappa, E. *Inorg. Chim. Acta* **1977**, *16*, L7. (b) Aime, S.; Milone, L.; Rossetti, R.; Stanghellini, P. L. *Inorg. Chim. Acta* **1977**, *22*, 135. (c) Band, E.; Muetterties, E. L. *Chem. Rev.* **1978**, *78*, 639. (d) Kegl, T.; Ungvary, F. *J. Organomet. Chem.* **2007**, *692*, 1825.

equatorial adduct **$Co_2(CO)_7$·TMAO-eq** will importantly predominate in solution ($\Delta E_{eq/ax} = -1.33$ kcal/mol).

The cleavage of the O−N bond in these adducts was next studied. In both cases, a transition state corresponding to the considered process could be located and characterized. In terms of activation energy, the most favorable situation corresponds to the cleavage of the equatorial adduct through **TS N-O cleavage-eq** ($\Delta E_{B3LYP} = 24.41$ kcal/mol). In geometrical terms, the cleavage processes are characterized by late transition states, as deduced from the small differences between the Co−O bond distances in the transition states and in the oxidized product **$Co_2O(CO)_7$**. From a thermodynamic point of view, the oxidation of **$Co_2(CO)_7$** to **$Co_2O(CO)_7$** mediated by TMAO is predicted to be essentially thermoneutral ($\Delta H_r = 3.13$ kcal/mol).

Thus, the present theoretical calculations are clearly indicative of the existence of a low-energy pathway for the oxidation of Co(0) to Co(II) mediated by amine oxides. Although the studied process admittedly represents an oversimplification of the possible steps involved in the conversion of $Co_2(CO)_8$ into CoO nanoparticles, the basic process of amine oxide addition, followed by N−O cleavage is most probably involved in the conversion.

Magnetic Behavior. As we have seen, the structural characterization by TEM of the materials arising from the amine oxide-induced decomposition of octacarbonyl dicobalt showed the existence of narrowly disperse, large aggregates made of individual, small CoO nanoparticles. This dual character of the material results in the observation of a clear bimodality in its magnetic properties, as determined by low susceptibility measurements (Figure 8).

The temperature dependence of the magnetization of the CoO particles prepared with amine oxides **1**−**3** was measured with the use of zero-field cooling (ZFC) and field cooling (FC) procedures in an applied magnetic field of 50 Oe between 2 and 50 K. The plots of temperature versus magnetization for the three different amine oxides are presented in Figure 8.

In contrast with the usual behavior of magnetic materials, which present in the ZFC curve a peak at the blocking temperature (T_B) of the sample, the studied samples present ZFC curves with two distinct peaks, at 4–7 and 14–16 K. Taking into account that, for a given material, $T_B$depends on particle size ($KV = k_B T_B$; where K is the anisotropy constant, V the particle volume, k_B the Boltzman constant, and T_B the blocking temperature); the presence of the two peaks suggests the presence of magnetic domains of two different sizes in the samples. The observed T_B values are consistent with those reported in the literature for nanoparticles of the same nature.[21]

Because TEM analysis only shows the presence in the sample of small (∼1.7 nm diameter) individual particles and larger (>100 nm diameter) aggregates thereof, we conclude that the observed peaks in these samples are caused by the individual particles ($T_B \approx$ 4–7 K) and the agglomerates ($T_B \approx$ 14–16 K). The magnetization in both the individual particles and in the aggregates has its origin in the uncompensated antiferromagnetic spins at the

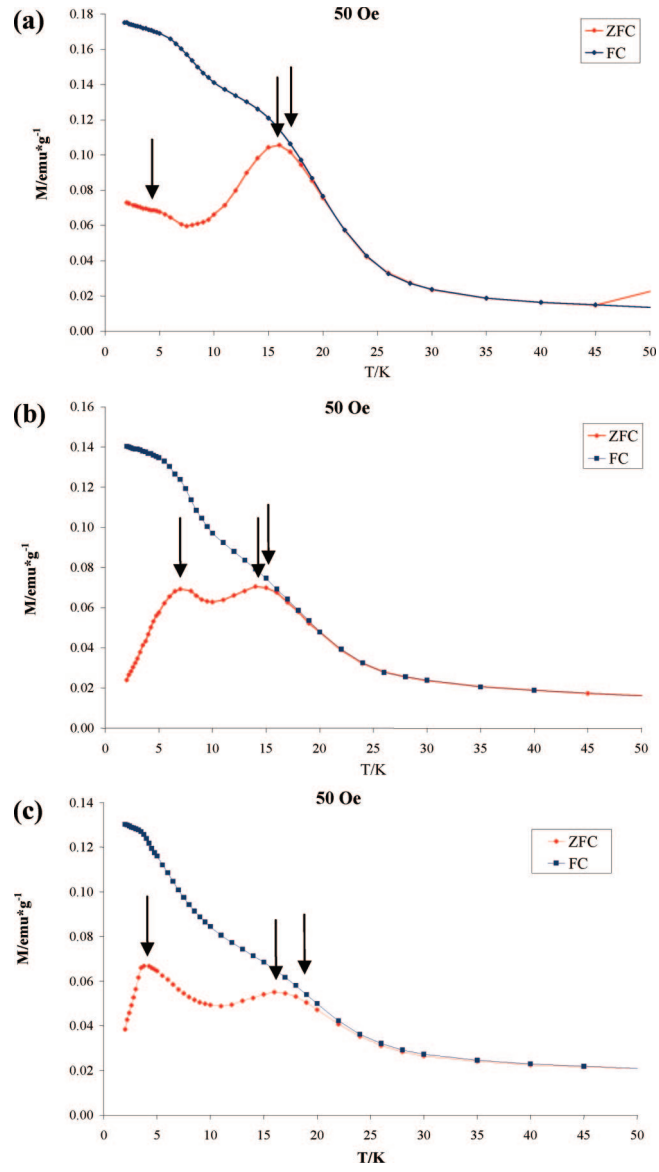

Figure 8. ZFC-FC curves measured at 50 Oe for CoO particles prepared using (a) NMO, (b) PPNO, and (c) DMONO as decarbonylation/oxidation promoters. The arrows indicate, at increasing temperature values, T_B for the individual particles, T_B for the aggregates, and T_{irr}, respectively.

nanoparticle surface.[36] In the case of the aggregates, the observed collective behavior is probably related to cooperative dipolar interactions, as previously observed,[37] and related to magnetic surface effects where the large magnetization present at the surfaces of single-domain materials could induce formation of larger and more magnetically responsive particles.[38] Such collective effects have not been observed until quite recently when, because of the development of wet chemical syntheses of nanoparticles, a high degree of size, shape, composition, and surface state control has been achieved. In fact, we observed simultaneously in each of our samples what has

(36) (a) Neel, L. *Compt. Rend.* **1961**, *252*, 4075. (b) Dormann, J. L.; Fiorani, D.; Tronc, E. *Adv. Chem. Phys.* **1997**, *98*, 283.
(37) Puntes, V. F.; Gorostiza, P.; Aruguete, D. M.; Bastus, N. G.; Alivisatos, A. P. *Nat. Mater.* **2004**, *3*, 263.
(38) Yavuz, C. T.; Mayo, J. T.; Yu, W. W.; Prakash, A.; Falkner, J. C.; Yean, S.; Cong, L.; Shipley, H. J.; Kan, A.; Tomson, M.; Natelson, D.; Colvin, V. L. *Science* **2006**, *314*, 964.

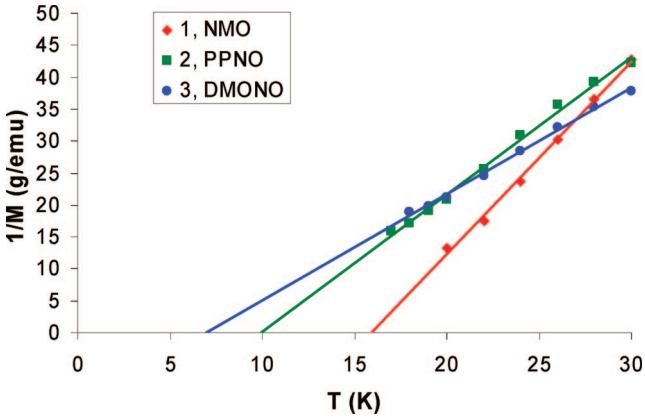

Figure 9. Linear parts of the inverse of magnetization vs *T* plot at 50 Oe for CoO nanoparticles prepared with *N*-oxides **1**−**3**.

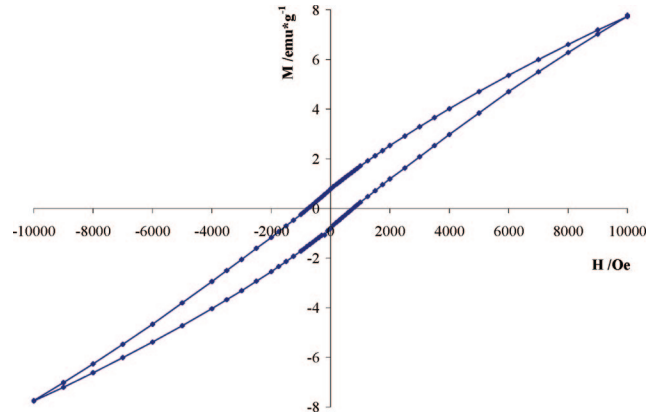

Figure 10. Hysteresis loops at 2 K for CoO NP prepared with NMO.

been previously observed in other systems with different samples, as in the case of Fe_3O_4,[39] where depending on the degree of order in the studied sample, the value of T_B (and the ZFC peak shape) varied accordingly.

Interestingly, the bimodal character can also be observed in the FC curves. An irreversible temperature, T_{irr}, at which the ZFC and FC curves split can be observed for each set of nanoparticles. This T_{irr} is related to the broadness of the magnetic size distribution and is located close to the highest T_B peak of the ZFC, indicating reasonable sample magnetic monodispersity. As it can be observed, depending on the oxidizing agent employed for the preparation, similar particles and aggregates are obtained (See Figures 3 and 4 and the Supporting Information); however, the relative intensity of the two peaks, the temperatures at which they appear, and the irreversible temperatures show slight differences from one another.

To observe the interactions between particles in the aggregates, the inverse of the magnetization at low fields was plotted versus temperature. The linear behavior was extrapolated to find out whether it goes to zero, positive, or negative values of *T*. In the case of non-interacting magnetic nanoparticles, the extrapolation should go to zero.[40] In the present case (Figure 9), the extrapolation of the linear regime gives positive values of *T* indicating the ferromagnetic-like character of the interactions of the nanoparticles inside the aggregates.

Hysteresis loops (Figure 10 and Supporting Information) show both the contribution of the antiferromagnetic core of CoO (a linear positive behavior passing through zero) and the existence of a ferromagnetic part (the hysteresis). As discussed above, the ferromagnetic part comes from the uncompensated spins at the nanoparticle surface[36] within the aggregate. The same behavior, that is, coexistence of ferromagnetic and antiferromagnetic phases, can be observed in the representation of the inverse of *M* versus *T* at 1 *T* (see Supporting Information), where the nature of the magnetic coupling between cobalt atoms (ferromagnetic, antiferromagnetic, or ferrimagnetic) can be inferred to follow a pure paramagnetic behavior between 50 and 300 K (superparamagnetic particles show a small curvature at such *T* regime).[36b] The downward departure from the paramagnetic behavior observed below 50 K is evidence of the formation of magnetic moments in the cobalt oxide nanoparticles, once the paramagnetic-ferromagnetic ordering is reached. The extrapolated temperature from the linear regime at $1/M$ gives a value of −50 K. This negative value also indicates antiferromagnetic coupling between cobalt atoms.

Conclusions

Pure CoO nanoparticles (∼1.7 nm diameter) have been prepared by a simple, low-temperature decarbonylation−oxidation method using amine oxides as oxidizers and oleic acid as stabilizing agent. The nanoparticles spontaneously agglomerate into spherical (*ca.* 110–160 nm diameter) aggregates. Of the different amine oxides tested, *N*-methylmorpholine *N*-oxide (NMO) turns out to be the most advantageous in terms of reaction rate, nanoparticle yield, and size/shape profile of the aggregate. The samples of nanoparticles prepared by this method exhibit an unusual magnetization versus temperature behavior, with two distinct peaks. These appear to be associated to the blocking temperatures of the individual nanoparticles and of magnetic domains in the spontaneously assembled aggregates.

The possibility of extending this methodology to other *N*-oxides and other metal–carbonyl precursors by adjusting experimental conditions is currently being investigated in our laboratories.

Acknowledgment. The authors thank Dr. L. Calvo for XPS measurements, Dr. J. Arbiol for EELS analysis, and J. Mendoza for technical assistance with TEM, all of them from Serveis Científico-Tècnics de la Universitat de Barcelona. A.L. thanks ICIQ Foundation for a fellowship. M.A.P. thanks Generalitat de Catalunya for the "Distinció per a la Promoció de la Recerca Universitària" award. Financial support from MEC (CTQ2005-

(39) Poddar, P.; Telem-Shafir, T.; Fried, T.; Markovich, G. *Phys. Rev. B* **2002**, *66*, 060403.
(40) Respaud, M.; Broto, J. M.; Rakoto, H.; Fert, A. R.; L; Thomas, L.; Barbara, B.; Verelst, M.; Snoeck, E.; Lecante, P.; Mosset, A.; Osuna, J.; Ould Ely, T.; Amiens, C.; Chaudret, B. *Phys. Rev. B* **1998**, *57*, 2925.

02193/BQU), DURSI (2005SGR225), Consolider Ingenio 2010 (Grant CSD2006-0003), and ICIQ Foundation is gratefully acknowledged.

Supporting Information Available: Experimental setup for in situ IR monitored decarbonylation, TEM micrographs paragraphs, XPS and EELS of CoO nanoparticles, hysteresis loops and inverse of magnetization versus temperature at high external field for CoO nanoparticles, and Cartesian coordinates of the calculated species. This information is available free of charge via the Internet at http://pubs.acs.org.

CM7018636